Faraday Discussions

Cite this: *Faraday Discuss.*, 2014, **171**, 259

PAPER

X-ray absorption spectroscopy with time-tagged photon counting: application to study the structure of a Co(I) intermediate of H_2 evolving photo-catalyst

Grigory Smolentsev,*[a] Alexander A. Guda,[b] Markus Janousch,[a] Cristophe Frieh,[a] Gaudenz Jud,[a] Flavio Zamponi,[c] Murielle Chavarot-Kerlidou,[d] Vincent Artero,[d] Jeroen A. van Bokhoven[ac] and Maarten Nachtegaal[a]

Received 7th March 2014, Accepted 14th April 2014
DOI: 10.1039/c4fd00035h

In order to probe the structure of reaction intermediates of photochemical reactions a new setup for laser-initiated time-resolved X-ray absorption (XAS) measurements has been developed. With this approach the arrival time of each photon in respect to the laser pulse is measured and therefore full kinetic information is obtained. All X-rays that reach the detector are used to measure this kinetic information and therefore the detection efficiency of this method is high. The newly developed setup is optimized for time-resolved experiments in the microsecond range for samples with relatively low metal concentration (~1mM). This setup has been applied to study a multicomponent photocatalytic system with a $Co(dmgBF_2)_2$ catalyst (dmg^{2-} = dimethylglyoximato dianion), $[Ru(bpy)_3]^{2+}$ chromophore (bpy = 2,2′-bipyridine) and methyl viologen as the electron relay. On the basis of the analysis of hundreds of Co K-edge XAS spectra corresponding to different delay times after the laser excitation of the chromophore, the presence of a Co(I) intermediate is confirmed. The calculated X-ray transient signal for a model of Co(I) state with a 0.14 Å displacement of Co out of the dmg ligand plane and with the closest solvent molecule at a distance of 2.06 Å gives reasonable agreement with the experimental data.

1 Introduction

Development of catalysts for hydrogen evolution from water using sunlight is a challenging task of great practical importance.[1,2] Molecular catalysts based on

[a]*Paul Scherrer Institut, WLGA 217, 5232, Villigen, Switzerland. E-mail: grigory.smolentsev@psi.ch; Tel: +41 56 310 5173*
[b]*Research Center for Nanoscale Structure of Matter, Southern Federal University, Sorge 5, 344090, Rostov-on-Don, Russia*
[c]*ETH Zurich, Wolfgang Pauli-Str. 10, 8093, Zurich, Switzerland*
[d]*Laboratory of Chemistry and Biology of Metals, Universite Grenoble Alpes, CEA, CNRS, France*

coordination complexes of 3d metals,[3,4] and especially cobalt,[5] have high potential for large-scale applications since they are earth-abundant in contrast to more robust platinum-based catalysts, that are more expensive and less abundant. The catalyst under investigation in the current contribution is $Co(dmgBF_2)_2$ (dmg^{2-} = dimethylglyoximato dianion)[6,7] (Scheme 1). Its hydrogen evolving activity in multicomponent systems in combination with different chromophores[8–10] and in supramolecular systems[8,9,11] has been investigated with several hundreds of turnovers achieved under homogeneous photocatalytic conditions in the presence of sacrificial electron donors. A few attempts have been made to improve the performance and stability by the modification of the Co ligands.[7,12,13] To fully exploit this approach and design ligands that stabilize the high energy intermediates along the catalytic pathway, detailed knowledge about the reaction mechanism is essential. Insights in the reaction mechanism can be gained on the basis of electrochemical[5] and steady-state physicochemical (*i.e.* UV-visible or EPR)[12,14–16] characterization coupled with quantum chemical calculations,[14,17,18] but tracking of certain intermediates is possible only using time-resolved spectroscopic techniques.

The key requirements to the techniques used to identify the photocatalytic intermediates are sensitivity to the structural and electronic changes of the catalytic center, selectivity that allows to distinguish the contribution of the catalyst from all other possible changes in the complicated chemical system and appropriate time range and resolution. Stopped flow and freeze quench methods are too slow to track the intermediates of H_2 evolving catalysts, especially for the most promising systems that produce hydrogen rapidly. Furthermore, since most of the reaction steps are intermolecular, the intermediates have lifetimes in the microsecond time range. Some initial reaction steps, for example, charge transfer from the chromophore to the catalytic center in the supramolecular systems can be intramolecular and occur within picoseconds,[19] but the charge-separated state has to be long lived to participate in the subsequent intermolecular reactions. Thus measurements in the microsecond range with sub-microsecond resolution are required for such applications.

Among time-resolved spectroscopic methods that are typically applied to study photocatalytic intermediates and reaction mechanism are transient optical absorption spectroscopy[20,21] and time-resolved IR.[22] Time-resolved X-ray absorption spectroscopy (XAS) has a few advantages in comparison with optical and IR methods. First of all XAS is element-specific and therefore the contribution from the metal center of the catalyst is separated from all other changes in the system. Second, XAS spectra contain structural information about the local arrangement of the metal (in the fine structure of the near edge X-ray absorption spectrum

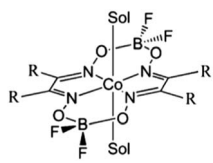

Scheme 1 Structure of $Co(dmgBF_2)_2$ (R = methyl) and $Co(dpgBF_2)_2$ (R = phenyl). Sol is a solvent molecule (CH_3CN).

known as XANES) and information about the oxidation state (mainly in the position of the absorption edge). Setups for time-resolved hard X-ray absorption spectroscopy measurements with ~100 ps resolution have been developed at a few beamlines worldwide.[23–28] Experiments in the microsecond range are quite rare and can be performed using spatially separated laser and X-ray beams (pump–flow–probe mode)[29,30] gating of the detector (pump–probe mode)[31] or recording the arrival time of all photons (pump–sequential-probes mode).[29,32–34]

Pump–flow–probe experiments use non-overlapping laser excitation and X-ray probing beams focused on the sample jet. The solution is circulating in the flow system and a cylindrical jet with a liquid speed of a few meters per second is formed. A continuous wave laser focused on the jet initiates the reaction, the distance between laser and X-ray beams and the velocity of the liquid flow determine the time delay, while the focusing of both beams defines the time resolution. The pump–flow–probe method is characterized by a high detection efficiency and the resolution is limited to ~40 μs with easily achievable flow parameters (flow speed ~5m s^{-1}, jet diameter ~1mm) and moderate X-ray spot size (~100 μm). Pump–probe experiments with a microsecond resolution can use the same data acquisition electronics as pump–probe experiments with picosecond resolution by increasing the width of the X-ray detector gate pulse. Since many X-ray bunches delivered by the synchrotron will fall within the time window defined by such a gate pulse, the time resolution is defined by the width of this pulse. The detection efficiency of pump–probe methods also depends on the gate, its shortening corresponds to higher time resolution but lower efficiency. Acquiring kinetic data with this approach requires scanning the delay between laser and gate pulses.

In the present manuscript we report a pump–sequential-probes setup to study photocatalytic intermediates that have lifetimes in the microsecond range. This setup is realized at the SuperXAS beamline of the Swiss Light Source and described in the experimental setup section. With this approach the arrival time of each photon in respect to the laser pulse is measured (method known as time-tagged photon counting) and therefore, in contrast to currently available pump–probe setups, full kinetic information is obtained without any delay scan. In the application section we demonstrate how this method is used to identify the intermediate states of a $Co(dmgBF_2)_2$ catalyst in the multicomponent system and to probe the structure of the Co(II) and Co(I) states of the catalyst in solution.

2 Experimental setup

X-ray source

The pump–sequential-probes setup has been developed and implemented at the SuperXAS beamline of the Swiss Light Source (SLS), Villigen, Switzerland. The X-ray beam was delivered by the 2.9 T super-bend magnet. The SLS was run in the standard top-up mode with an average current of 400 mA. A collimated beam was formed by means of a Si mirror and the energy has been scanned by a channel-cut Si(111) monochromator. A toroidal mirror with Rh coating was employed after the monochromator to focus the incident X-rays with a spot size of 100 × 100 μm^2 on the sample. The photon flux obtained with this configuration at the sample was about 3.2 × 10^{11} photons/s.

Laser source

For time-resolved experiments the optimal repetition rate of the laser can be chosen maximizing the efficiency of X-ray flux usage. A useful X-ray signal of the excited state is obtained first of all during the time when intermediate species are formed in the detectable amount. Since the difference between excited and unexcited spectra is measured, the system has to fully return to the initial state between laser pulses. Therefore approximately half of the laser period can be used to measure the ground state contribution. As the result, the optimal repetition rate corresponds to a few lifetimes of the studied intermediate. Nevertheless if such species live too long or if the lifetime is not known *a priori* it is necessary to refresh the sample between two subsequent laser pulses. For samples in the liquid phase this can be achieved using a liquid jet flow system which is also beneficial to reduce X-ray and laser induced damage of the sample. In such a configuration, the period of the laser should not be much longer than the time required to refresh the sample. The second factor that has to be taken into account is the laser pulse energy that usually decreases with increasing repetition rate and must be sufficient to efficiently excite the sample.

For our source, the maximal focusing of the X-ray beam is $\sim$100 $\times$100 μm^2. The laser spot with diameter D has to be bigger in order to probe only the volume excited efficiently and taking into account that it is difficult to achieve a stable flow of the sample in the liquid jet with a speed v higher than $\sim$5m s^{-1}, the maximal repetition rate $f = v/D \sim 30$ kHz is required. In our setup we used a Xiton IDOL laser with a repetition rate up to 40 kHz and maximal output power $\sim$2W at 15kHz. Available wavelengths for this laser are 447 nm and 671 nm. Maximal pulse energy is 125 μJ which is more than enough to excite samples of reasonable optical density (0.2 or higher) with a metal concentration of $\sim$1 mM in an irradiated volume of $\sim$200 μm diameter and $\sim$1 mm thickness.

Data acquisition system (DAQ)

The main advantage of our DAQ is the use of the so-called time-tagged single photon counting method to obtain kinetic and structural information from XAS in the range between tens of nanoseconds up to hundreds of microseconds. Such an approach allows us to use the flux of a bending-magnet beamline efficiently. The setup (see Fig. 1) is based on the multichannel digital X-ray processor XIA XMAP running in the so-called list mapping mode. In this regime information about each registered photon (arrival time, with respect to the trigger with a precision of 20ns, and energy) is buffered and then saved to file in HDF5 format. As detectors for incoming and fluorescence radiation we used avalanche photo diodes (APDs) coupled to the charge sensitive preamplifier. An additional APD that is sensitive to the laser light is connected to one of the channels of the digital X-ray processor and provides the reference signal of the timing of the laser pulse.

To achieve synchronization between X-rays, laser and DAQ we used the radio frequency (RF) signal from the storage ring (500 MHz), which is intrinsically synchronized with the X-ray pulses. It serves as the input for the event receiver (Micro Research, VME-EVR-230RF) that divides the frequency of the RF signal and generates square pulses corresponding to the required repetition rate of the experiment. These signals are further processed with the delay card (Micro Research, 4CHTIM-200) generating pulses of required duration (2 μs for the laser

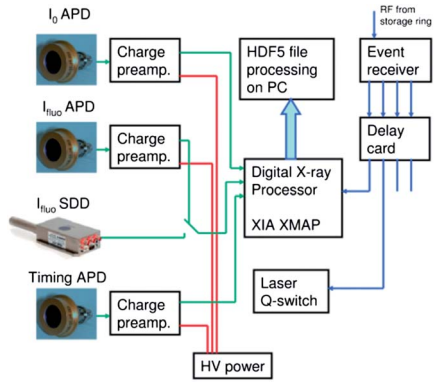

Fig. 1 Scheme of the data acquisition system for the pump–sequential-probes experiments.

trigger, 40ns for the digital X-ray processor trigger) and with required relative delay. The signal sent to the laser allows to control its acousto-optic modulator and thus to achieve synchronization between the actual laser pulse and DAQ better than 2 ns. HDF5 files generated by XMAP are processed online during the incoming X-ray energy scan with a short delay (time of measurement of 1–2 energy points). Histograms with the number of events as a function of time for selected energies of fluorescent photons are calculated. Further processing such us calculation of transient spectra is performed on the basis of these data.

Synchronization

The distribution of the current in synchrotron storage rings is not uniform and at the SLS a hybrid mode is often used. 390 bunches are separated by 2 ns from each other and they form the multibunch train while one additional more intense pulse, the so-called camshaft is located in the gap between multibunches (Fig. 2). While such a distribution is useful for experiments that require a 100 ps time resolution correlated to the width of the camshaft pulse,[35] a uniform average incoming intensity distribution is preferable for microsecond and nanosecond experiments. This has been achieved by keeping the synchronization between laser and DAQ and simultaneously shifting these two triggers relatively to the filling pattern of the synchrotron. This mode of our experimental setup we call asynchronous. Schematically it is shown in Fig. 2.

After each laser pulse intensities I_0 and I_f are measured as a function of time. A spectrum with good statistics can be obtained by averaging X-ray data following at least 10^5 laser pulses. However if the time position of the laser pulse is fixed to the camshaft position, the I_0 as a function of time would exhibit dips in intensity, as shown in Fig. 2 by I_0 synch. Instead, in the asynchronous mode the trigger pulses follow with the frequency so that the filling pattern of the storage ring is shifted relative to the laser pulse by 2 ns (1/480 of the storage ring cycle) after each laser period. As a result measuring each point of the spectrum for at least 10 s (corresponding to 10^4 laser cycles) one observes a uniform intensity distribution for the incoming beam, as shown in Fig. 2 by I_0 asynch. It allows to avoid "bad time points" that correspond to the measurements of the kinetic histogram during the

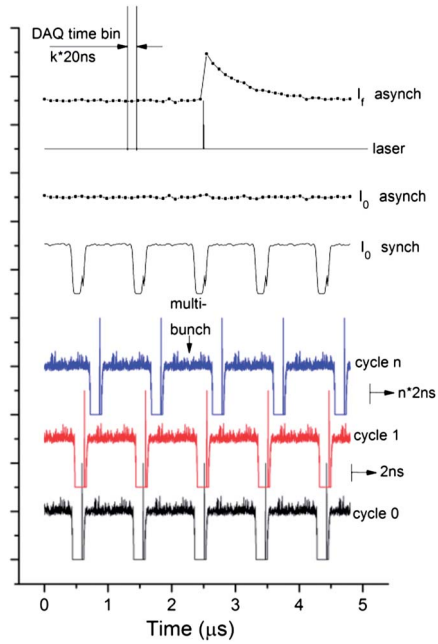

Fig. 2 Scheme of measurements using the synchronous and asynchronous modes of data acquisition system. Distribution of incoming X-ray intensity as a function of time is shown for a few individual cycles and for the averaged intensity in the synchronous and asynchronous mode. Position of the laser pulse and averaged intensity for the fluorescent detector are also shown.

time between multibunches of the storage ring. Additionally, we eliminated the need of incoming intensity measurements for each time point $I_0(t)$. Only the average value I_0 has to be measured. In the synchronized mode fluorescence intensity has to be normalized to the incoming intensity for each time point since bunches in the storage ring have a different current. Simplification of I_0 detection in the asynchronous mode has a positive impact on the signal to noise ratio of measured XAS spectra since the contribution of noise from I_0 measurements becomes negligible.

Detectors

Large area avalanche photo diodes (Advanced Photonix Inc, model 630-70-72-500) with a 200 mm^2 sensitive surface area and a ~400 μm sensor thickness were used as detectors. Rise time of signal from APD after the charge preamplifier (fast-ComTec, model CSP10) was measured and it is 30–40 ns (10–90%), depending on the device. The overall time resolution of the setup (that takes into account the contribution from the finite sampling frequency of the digital X-ray processor, APD and preamplifier contributions and all other synchronization jitters) is 30 ns (FWHM) as measured with only one bunch in the storage ring. The energy resolution of APDs is 700–800 eV at 5.9 keV which is not sufficient to discriminate efficiently the elastic scattering of X-rays and sample fluorescence. Therefore we used the combination of a Z-1 filter to reduce the unwanted background from the

elastically scattered photons and Soller slits with conical geometry that partially protect the detector from re-fluorescence from the Z-1 filter. The distance between slit and the sample jet was fixed at 6 mm. The geometrical parameters of the slit were optimized numerically by finding a compromise between the efficiency of the slit and the minimization of the distance between sample and detector. Longer slits block re-fluorescence more efficiently, but the solid angle for the detector becomes smaller. As a result we have constructed a Soller slit with a 5.6 mm thickness that has an efficiency $\gamma = 0.962$ (only 3.8% of re-emitted photons will find a way to the detector) and with slit transmittance of 78% (22% of useful fluorescence photons will be blocked by the slit). Our DAQ is also compatible with silicon drift detectors that have lower time resolution and area, but at the same time have higher energy resolution and therefore can be used without Z-1 filter and Soller slits.

Samples

$[Ru(bpy)_3]Cl_2$, methyl viologen dichloride ($MVCl_2$), NH_4PF_6, NBu_4PF_6 and anhydrous acetonitrile were purchased from Sigma-Aldrich and used without further purification. As photo-sensitizer and electron-relay, $[Ru(bpy)_3](PF_6)_2$ and $MV(PF_6)_2$ were prepared from NH_4PF_6 and $[Ru(bpy)_3]Cl_2$ or $MVCl_2$, respectively, following a standard anion-exchange procedure. The catalyst $[Co(dmgBF_2)_2(OH_2)_2]$ (dmg^{2-} = dimethylglyoximato dianion) was purchased from Strem Chemicals Inc. The sample consisted of an acetonitrile solution of $[Ru(bpy)_3](PF_6)_2$ (0.4 mM), $MV(PF_6)_2$ (8 mM), tetrabutylammonium hexafluorophosphate NBu_4PF_6 (0.1M) and $[Co(dmgBF_2)_2(CH_3CN)_2]$ (0.8 mM), which forms spontaneously from $[Co(dmgBF_2)_2(OH_2)_2]$ in CH_3CN solution. The solid-state metal complexes were handled in air. The freshly prepared sample solution was degassed with N_2 at least 30 min before the experiment and continuously purged and kept under N_2 during the experiment.

3 Theoretical method

Calculations of XANES spectra were performed using the full multiple scattering approach realized in the FEFF8 code.[36] The self-consistent potential within the muffin-tin approximation has been calculated for the cluster with a 4.9 Å radius. The energy-dependent exchange-correlation potential is obtained from the Hedin-Lundqvist approach. A cluster with radius 4.9 Å was also used for full multiple scattering calculations of spectra.

4 Application

The method has been applied for preliminary studies of the charge transfer in the multicomponent photo-catalytic system which consists of $Co(dmgBF_2)_2$ catalyst, $Ru(bpy)_3^{2+}$ chromophore and methyl viologen (MV^{2+}) that acts as the electron relay. This system was inspired from a similar study by Gray and coworkers using a $Co(dpgBF_2)_2$ catalyst (dpg^{2-} = diphenylglyoximato dianion) instead of $Co(dmgBF_2)_2$.[21] The initial Co species has a formal oxidation state of 2+. After photo-excitation of the chromophore the following reactions steps are hypothetically possible:

$$[Ru(bpy)_3]^{2+*} + MV^{2+} \rightarrow [Ru(bpy)_3]^{3+} + MV^{+}$$

$$[Ru(bpy)_3]^{2+*} + Co(II) \rightarrow [Ru(bpy)_3]^{3+} + Co(I)$$

$$MV^{+} + Co(II) \rightarrow Co(I) + MV^{2+}$$

$$[Ru(bpy)_3]^{3+} + Co(II) \rightarrow [Ru(bpy)_3]^{2+} + Co(III)$$

According to the time-resolved optical data reported for $Co(dpgBF_2)_2$[21] the catalyst in the Co(III) state is formed in parallel with Co reduction at the conditions without any proton source. In most Co-based H_2-evolution systems,[5] Co(I) species play a crucial role in the catalytic mechanism: protonation of Co(I) yields Co-hydride intermediates which are the actual active species involved in H_2 evolution, either in the Co(III)-H state or in the Co(II)-H state obtained after a subsequent reducing event.

Our first goal has been to determine how many Co intermediates formed in the system. In the bottom panel of Fig. 3 we show the transient signal corresponding to different delay times between laser pump and registered X-ray photons. The width of the time window for the data corresponding to the long delay is significantly larger than for other two spectra to compensate the reduction of statistics due to the signal reduction, one can also notice that the data measured for the (0.25, 0.75) μs delay is noisier than the spectrum corresponding to a six times wider (−0.25, 2.75) μs time window. The amplitude of the transients has been renormalized for easier comparison. The time-dependence of the signal monitored at a fixed X-ray energy corresponding to the maximum of the transient signal is shown in the top panel of Fig. 3. Since a liquid jet with continuous flow has been used to refresh the sample between two laser pulses the slow component of the decay can be caused by the movement of the excited volume out of the probed area, while the quick decay of the signal during the first 20 μs is related to the real kinetics of the system. Kinetic measurements utilizing the flow system are thus not as precise as those that one can imagine in the experiment with the full exchange of the sample during the pause before each laser pulse (the repetition rate of such measurements will be extremely low). Nevertheless, the experimental spectra (bottom panel of Fig. 3) measured at different time delays have very similar shapes indicating the formation of only one novel species upon irradiation of the photocatalytic system. The same result has been obtained from the analysis of the shape of the transient signals as a function of time over a set of 200 experimental spectra using the method reported in ref. 37, which indicated the presence of only 2 independent spectral components in our data corresponding to the initial species together with one intermediate species.

Fig. 4 shows the experimental XANES spectrum of the photocatalytic system measured before the laser pulse together with the transient spectrum that corresponds to the 10 μs time window after the laser pulse. The position of the absorption edge of the intermediate species is shifted towards lower energies with regards to the initial Co(II) (first peak of the transient signal is positive), indicative of the formation of a more reduced species, likely the Co(I) intermediate mentioned above and expected to be the entry point into a catalytic cycle for H_2 evolution.

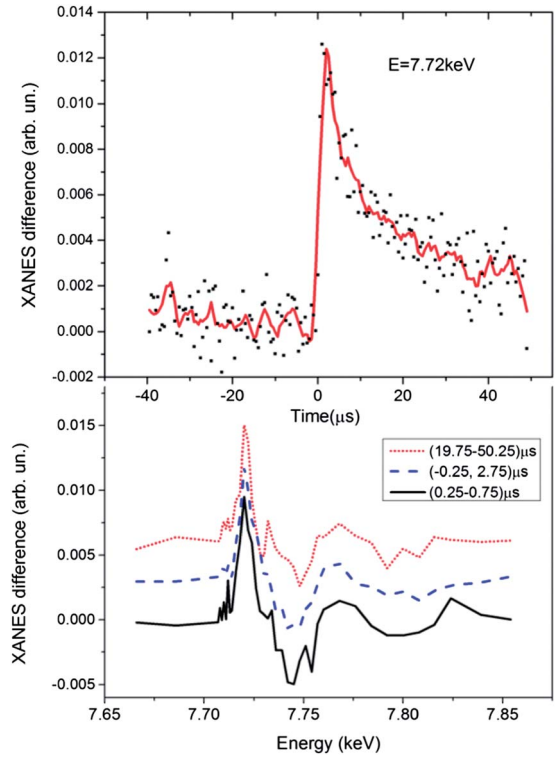

Fig. 3 Top Panel: Transient XANES signal measured for fixed energy of the incoming X-ray beam (E = 7.72keV) as a function of time between laser pump and X-ray probe. Bottom: Transient XANES spectra corresponding to different time windows after the laser pulse: (0.25, 0.75) μs, black line; (−0.25, 2.75) μs, blue line and (19.75, 50.25) μs, red line. Amplitudes were re-normalized for a better comparison.

The local structure around the metal center for molecules in solution can differ from that in the crystal phase measured using XRD and from that obtained by DFT optimization in vacuum. This is especially true for metal complexes possessing vacant coordination sites or labile ligands. $Co(dmgBF_2)_2$ belongs to this class of metal complexes and therefore we have started the simulations from the refinement of the structure of the initial Co(II) state. Both XRD[38] and DFT[17] structures of $[Co(dmgBF_2)_2(CH_3CN)_2]$ have rather distant solvent molecules with bond lengths of 2.25 Å and 2.33 Å correspondingly, while some other Co(II) complexes with distorted octahedral environment and acetonitrile in the first coordination shell have significantly shorter $Co–N_{Sol}$ bonds (2.08–2.09 Å) in the crystallized state.[39,40] Therefore in addition to XRD and DFT structures we have constructed models (3) and (4) with short $Co–N_{Sol}$ bonds (2.06 Å and 2.0 Å respectively). To take into account the expected disorder of the solvent molecules and avoid biases due to the strong multiple scattering along the Co–*N*–C path as found in the crystal and DFT-based structures, we have approximated the contribution of solvent to the XANES by taking into account the scattering from the nearest N atoms only.

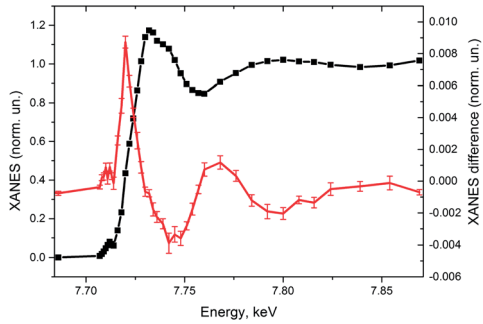

Fig. 4 Co K-edge XANES of the multicomponent photocatalytic system with $Co(dmgBF_2)_2$ catalyst in the ground state (black line, left scale) and transient X-ray absorption spectrum (red line, right scale) that corresponds to 10 μs time window after the laser pulse.

Fig. 5 shows that the agreement between the experimental spectrum and the spectra calculated for XRD (1) and DFT (2) models is not satisfactory. The relative intensity of peaks B and C is wrong. In addition, both calculated spectra display a shoulder between minimum D and maximum E that is not so well pronounced in the experimental data. Both models with short Co–N_{Sol} bonds (3 and 4) agree reasonably well with the experiment. Variation of the Co–N_{Sol} distance within these limits influences slightly the intensity of shoulder A which is observable, but rather weak in the experimental spectrum. As an additional small adjustment we have reduced the Co–N_{eq} distances for models (3) and (4) by 0.03 Å relative to the XRD model. It has not changed the overall shape of the spectrum but has allowed to achieve a better agreement in the position of minimum D.

Experimentally determined reference structures for Co(I) species with glyoxime ligands are very rare in the literature. The only available crystal structure of a Co(I) complex with 2 diphenylglyoximato ligands and acetonitrile has been reported in ref. 12. Since the atomic cluster with radius 4.9 Å has been used to calculate X-ray absorption spectra, the substitution of methyl by phenyl group does not influence significantly the shape of XANES. According to this XRD model Co(I) is five-coordinated in a distorted square-pyramidal environment with a short 1.97 Å Co–N_{Sol} bond and 0.27 Å displacement of Co out of the plane formed by the equatorial nitrogen atoms. Acetonitrile is oriented almost perpendicularly to the equatorial plane with a Co–*N*–C angle of 174°. Hu *et al.* note that "solvent molecules were severely disordered and could not be refined accurately".[12] The DFT optimized structure for Co(I) state reported by Muckerman and Fujita[17] has a significantly different orientation of the solvent molecules. Two of them were included in this model and the authors have found that both of them are oriented by the CH_3 group towards the Co atom with large Co–C distances of 3.7 Å and 4.8 Å, thus the Co atom is 4-coordinated.

Model (3) of the Co(I) intermediate has been constructed starting from the model of the Co(II) species with disordered solvents (curve (3) in Fig. 5) that gave a good agreement with the experiment. One of the solvent molecules has been moved away from the Co center to the distance 2.18 Å, while the second CH_3CN has been fixed at 2.06 Å. Additionally we have introduced a moderate out of plane

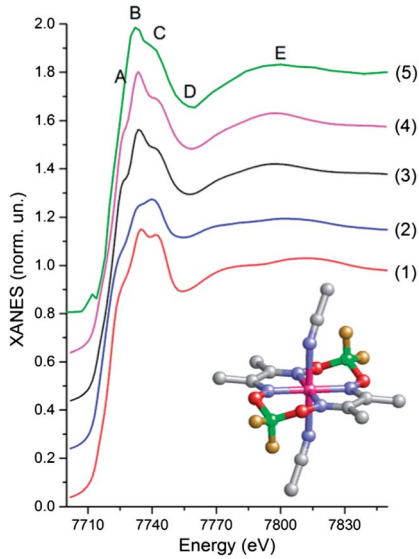

Fig. 5 Theoretical Co K-edge XANES spectra of $[Co^{II}(dmgBF_2)_2(CH_3CN)_2]$ calculated for a model obtained using either X-ray diffraction[38] (red curve (1)), DFT optimization[17] (blue curve (2)), a model with disordered solvent molecules with Co–N_{Sol} distances of 2.06 Å (black curve (3)) and 2.00 Å (magenta curve (4)). Curve (5) is the experimental spectrum of the multicomponent photocatalytic system with $[Co(dmgBF_2)_2(CH_3CN)_2]$ catalyst measured before the laser pulse. The insert shows the structure of $[Co(dmgBF_2)_2(CH_3CN)_2]$. Grey atoms are C, red O, blue N, green B, yellow F, magenta Co. H atoms are omitted for simplicity.

displacement of the Co atom (0.14 Å) and a small contraction of Co–N_{eq} (0.02 Å) as it has been suggested in both XRD and DFT models. Fig. 6 compares theoretical transient spectra calculated for these three models with the experimental pump–probe data. In addition to the structural changes we have taken into account 1 eV chemical shift of the absorption edge which is due to the movement of the core level as a result of changes of the screening by valence electrons. As one can see the shape of the transient signal is completely wrong for XRD model (1). The reason is similar to those observed also for the XRD structure of the ground state Co(II) species. Strong multiple scattering from the collinear Co–*N*–C chain of the solvent molecule influences the XANES significantly and therefore the model that ignores the disorder of solvent molecule fixing the solvent at idealized orthogonal orientation is not realistic. The DFT model is in better agreement with the experiment. A correct overall trend of the transient spectrum is seen, but all the main features are shifted in energy. Please note that even if the absolute scale of the energy calculations is not always correct we have performed already a few eV shift of the ground state spectrum and therefore there is no additional free parameter related with the independent shift of the transient spectrum. Among the 3 considered structures, model (3) gives the best agreement with the experiment. The theoretical spectrum is more structured between maxima A and B, which can be partially due to the fact that for the ground state peak A is more visible in the theory then in the experimental spectrum. Further improvement of

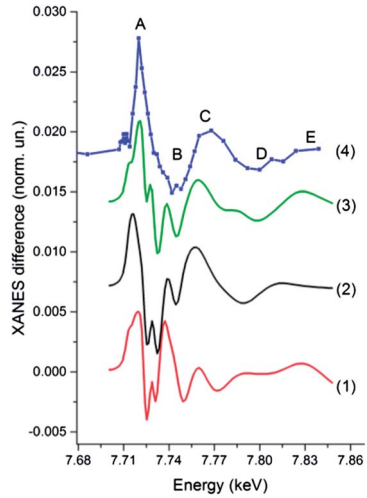

Fig. 6 Transient X-ray absorption spectrum corresponding to the transition from the Co(II) to Co(I) state. Calculations for different models of Co(I) state based on XRD (red curve (1), DFT (black curve (2)) and model with moderate out of plane displacement of Co and disordered solvent molecule (green curve (3)) are compared with the experimental data for the multicomponent photocatalytic system with $Co(dmgBF_2)_2$ catalyst (blue curve 4).

the theoretical model can be based on more accurate modeling of disordered solvent around the metal complex by averaging many configurations of solvent molecules, for example using the approach previously proposed in ref. 41. Nevertheless, on the basis of our data we can conclude that the model with disordered solvent molecules with the shortest Co–N_{Sol} distance ~2.06 Å and moderate displacement of Co out of the plane formed by N atoms of dmg ligands is the most realistic while the formation of a complex with perpendicular orientation of acetonitrile molecules has not been confirmed.

Discussing the experimental results shown in Fig. 4 that are plotted with the error bars we would like to mentioned that these measurements were taken during ~11 h and as one can see we have obtained a transient signal of very high quality. Please note that in comparison to the supramolecular systems,[42,43] or simple chromophorores,[44–46] the pump–probe signal for multicomponent systems is ~10 times weaker even if we are not limited by the pulse energy of the initial photoexcitation. Nevertheless, intermediates are relatively long-lived which somehow compensates the decrease of the statistics from the reduction of the signal amplitude. The incoming intensity of X-ray radiation at the bending magnet beamline of SLS is lower than, for example, at the undulator beamlines of the APS synchrotron. Paradoxically it can be seen also as an advantage since lower intensity allows to increase the detection efficiency using the single photon counting approach and at the same time to decrease the X-ray induced damage of the sample. In our previous work on the multicomponent system with similar Co-based catalyst that has been performed at 11ID-D beamline of the APS we observed a significant damage of the sample due to X-rays (incident X-ray flux $\sim 6 \times 10^{12}$ photons s^{-1}) while it was negligible at the SuperXAS beamline of the SLS (flux 3×10^{11} photons s^{-1}).[29] The number of photons registered by the

fluorescence detector at the APS is around 3–4 per X-ray bunch for the samples with ~1mM concentration; therefore single photon counting is not possible and the data acquisition system works in the current mode. At SuperXAS of SLS for analogous sample we have a bit less than 1 photon μs^{-1} and therefore single photon counting is efficient. An additional advantage of our approach that has not been used for the present application of the setup is the possibility to use energy-resolving detectors, such as silicon drift detectors, that have a resolution of ~120 eV and therefore allow for a further increase of the signal to noise ratio for diluted samples.

Acknowledgements

L. X Chen, X. Zhang and V. Sundstrom are acknowledged for constructive discussion. This work was supported by the Swiss National Science Foundation (grant no. 200021-135226), the European Commission's Seventh Framework Programme (FP7/2007-2013) under grant agreement no. 290605 (COFUND: PSI-FELLOW), the French National Research Agency (ANR, Labex program ARCANE, ANR-11-LABX-0003-01) and the European Research Council (ERC grant agreement no. 306398). The COST Action CM1202 PERSPECT-H2O is also acknowledged. AG would like to thank Russian Foundation for Basic Research (project #14-02-31555).

References

1 A. Thapper, S. Styring, G. Saracco, A. W. Rutherford, B. Robert, A. Magnuson, W. Lubitz, A. Llobet, P. Kurz, A. Holzwarth, S. Fiechter, H. de Groot, S. Campagna, A. Braun, H. Bercegol and V. Artero, *Green*, 2013, **3**, 43–57.
2 N. S. Lewis and D. G. Nocera, *Proc. Natl. Acad. Sci. U. S. A.*, 2006, **103**, 15729–15735.
3 W. T. Eckenhoff and R. Eisenberg, *Dalton Trans.*, 2012, **41**, 13004–13021.
4 V. S. Thoi, Y. Sun, J. R. Long and C. J. Chang, *Chem. Soc. Rev.*, 2013, **42**, 2388–2400.
5 V. Artero, M. Chavarot-Kerlidou and M. Fontecave, *Angew. Chem., Int. Ed.*, 2011, **50**, 7238–7266.
6 C. Baffert, V. Artero and M. Fontecave, *Inorg. Chem.*, 2007, **46**, 1817–1824.
7 X. Hu, B. M. Cossairt, B. S. Brunschwig, N. S. Lewis and J. C. Peters, *Chem. Commun.*, 2005, 4723–4725.
8 A. Fihri, V. Artero, A. Pereira and M. Fontecave, *Dalton Trans.*, 2008, 5567–5569.
9 A. Fihri, V. Artero, M. Razavet, C. Baffert, W. Leibl and M. Fontecave, *Angew. Chem., Int. Ed.*, 2008, **47**, 564–567.
10 P. Du, J. Schneider, G. Luo, W. W. Brennessel and R. Eisenberg, *Inorg. Chem.*, 2009, **48**, 4952–4962.
11 C. Li, M. Wang, J. Pan, P. Zhang, R. Zhang and L. Sun, *J. Organomet. Chem.*, 2009, **694**, 2814–2819.
12 X. Hu, B. S. Brunschwig and J. C. Peters, *J. Am. Chem. Soc.*, 2007, **129**, 8988–8998.
13 P. Zhang, P.-A. Jacques, M. Chavarot-Kerlidou, M. Wang, L. Sun, M. Fontecave and V. Artero, *Inorg. Chem. Commun.*, 2012, **26**, 51.

14 A. Bhattacharjee, M. Chavarot-Kerlidou, E. S. Andreiadis, M. Fontecave, M. J. Field and V. Artero, *Inorg. Chem.*, 2012, **51**, 7087–7093.
15 E. Szajna-Fuller and A. Bakac, *Eur. J. Inorg. Chem.*, 2010, 2488–2494.
16 T. Lazarides, T. McCormick, P. Du, G. Luo, B. Lindley and R. Eisenberg, *J. Am. Chem. Soc.*, 2009, **131**, 9192–9194.
17 J. T. Muckerman and E. Fujita, *Chem. Commun.*, 2011, **47**, 12456–12458.
18 B. H. Solis and S. Hammes-Schiffer, *Inorg. Chem.*, 2011, **50**, 11252–11262.
19 B. S. Veldkamp, W.-S. Han, S. M. Dyar, S. W. Eaton, M. A. Ratner and M. R. Wasielewski, *Energy Environ. Sci.*, 2013, **6**, 1917–1928.
20 J. L. Dempsey, J. R. Winkler and H. B. Gray, *J. Am. Chem. Soc.*, 2010, **132**, 16774–16776.
21 J. L. Dempsey, J. R. Winkler and H. B. Gray, *J. Am. Chem. Soc.*, 2010, **132**, 1060–1065.
22 B. Probst, C. Kolano, P. Hamm and R. Alberto, *Inorg. Chem.*, 2009, **48**, 1836–1843.
23 L. X. Chen, X. Zhang, J. V. Lockard, A. B. Stickrath, K. Attenkofer, G. Jennings and D. J. Liu, *Acta Crystallogr., Sect. A: Found. Crystallogr.*, 2010, **66**, 240–251.
24 C. Bressler and M. Chergui, *Annu. Rev. Phys. Chem.*, 2010, **61**, 263–282.
25 T. Sato, S. Nozawa, K. Ichiyanagi, A. Tomita, M. Chollet, H. Ichikawa, H. Fujii, S. Adachi and S. Koshihara, *J. Synchrotron Radiat.*, 2009, **16**, 110–115.
26 A. M. March, A. Stickrath, G. Doumy, E. P. Kanter, B. Krässig, S. H. Southworth, K. Attenkofer, C. A. Kurtz, L. X. Chen and L. Young, *Rev. Sci. Instrum.*, 2011, **82**, 073110.
27 M. Tromp, A. J. Dent, J. Headspith, T. L. Easun, X.-Z. Sun, M. W. George, O. Mathon, G. Smolentsev, M. L. Hamilton and J. Evans, *J. Phys. Chem. B*, 2013, **117**, 7381–7387.
28 E. A. Stern, D. L. Brewe, K. M. Beck, S. M. Heald and Y. Feng, *Phys. Scr.*, 2005, 1044.
29 G. Smolentsev, A. Guda, X. Zhang, K. Haldrup, E. S. Andreiadis, M. Chavarot-Kerlidou, S. E. Canton, M. Nachtegaal, V. Artero and V. Sundstrom, *J. Phys. Chem. C*, 2013, **117**, 17367–17375.
30 D. J. Thiel, P. Līviņš, E. A. Stern and A. Lewis, *Nature*, 1993, **362**, 40–43.
31 H. Wang, G. Peng and S. P. Cramer, *J. Electron Spectrosc. Relat. Phenom.*, 2005, **143**, 1–7.
32 E. M. Scheuring, W. Clavin, M. D. Wirt, L. M. Miller, R. F. Fischetti, Y. Lu, N. Mahoney, A. Xie, J. Wu and M. R. Chance, *J. Phys. Chem.*, 1996, **100**, 3344–3348.
33 A. B. Stickrath, M. W. Mara, J. V. Lockard, M. R. Harpham, J. Huang, X. Zhang, K. Attenkofer and L. X. Chen, *J. Phys. Chem. B*, 2013, **117**, 4705–4712.
34 M. Haumann, P. Liebisch, C. Muller, M. Barra, M. Grabolle and H. Dau, *Science*, 2005, **310**, 1019–1021.
35 F. A. Lima, C. J. Milne, D. C. V. Amarasinghe, M. H. Rittmann-Frank, R. M. van der Veen, M. Reinhard, V.-T. Pham, S. Karlsson, S. L. Johnson, D. Grolimund, C. Borca, T. Huthwelker, M. Janousch, F. van Mourik, R. Abela and M. Chergui, *Rev. Sci. Instrum.*, 2011, **82**, 063111.
36 A. L. Ankudinov, B. Ravel, J. J. Rehr and S. D. Conradson, *Phys. Rev. B: Condens. Matter Mater. Phys.*, 1998, **58**, 7565.
37 G. Smolentsev, G. Guilera, M. Tromp, S. Pascarelli and A. V. Soldatov, *J. Chem. Phys.*, 2009, **130**, 174508.

38 J. Niklas, K. L. Mardis, R. R. Rakhimov, K. L. Mulfort, D. M. Tiede and O. G. Poluektov, *J. Phys. Chem. B*, 2012, **116**, 2943–2957.
39 J. P. Bigi, T. E. Hanna, W. H. Harman, A. Chang and C. J. Chang, *Chem. Commun.*, 2010, **46**, 958–960.
40 C. C. Lu, E. Bill, T. Weyhermüller, E. Bothe and K. Wieghardt, *Inorg. Chem.*, 2007, **46**, 7880–7889.
41 P. D'Angelo, O. M. Roscioni, G. Chillemi, S. Della Longa and M. Benfatto, *J. Am. Chem. Soc.*, 2006, **128**, 1853–1858.
42 S. E. Canton, X. Zhang, J. Zhang, T. B. van Driel, K. S. Kjaer, K. Haldrup, P. Chabera, T. Harlang, K. Suarez-Alcantara, Y. Liu, J. Pérez, A. Bordage, M. Pápai, G. Vankó, G. Jennings, C. A. Kurtz, M. Rovezzi, P. Glatzel, G. Smolentsev, J. Uhlig, A. O. Dohn, M. Christensen, A. Galler, W. Gawelda, C. Bressler, H. T. Lemke, K. B. Møller, M. M. Nielsen, R. Lomoth, K. Wärnmark and V. Sundström, *J. Phys. Chem. Lett.*, 2013, **4**, 1972–1976.
43 G. Smolentsev, S. E. Canton, J. V. Lockard, V. Sundstrom and L. X. Chen, *J. Electron Spectrosc. Relat. Phenom.*, 2011, **184**, 125–128.
44 W. Gawelda, M. Johnson, F. M. F. de Groot, R. Abela, C. Bressler and M. Chergui, *J. Am. Chem. Soc.*, 2006, **128**, 5001–5009.
45 G. Smolentsev, A. V. Soldatov and L. X. Chen, *J. Phys. Chem. A*, 2008, **112**, 5363–5367.
46 L. X. Chen, W. J. Jager, G. Jennings, D. J. Gosztola, A. Munkholm and J. P. Hessler, *Science*, 2001, **292**, 262–264.